Investigation of CdTe, GaAs, Se and Si as Sensor Materials for Mammography

Simon Procz, Gerardo Roque, Carlos Avila, Jorge Racedo, *Student Member, IEEE*, Roberto Rueda, Ivan Santos, and Michael Fiederle

***Abstract*— Despite the benefits of mammography investigations, some studies have shown that X-ray exposure from the mammography screening itself can statistically cause breast cancer in a small fraction of women. Therefore, a dose reduction in mammography is desirable. At the same time, there is a demand for a higher spatial resolution in mammographic imaging. The most promising way to achieve these goals is the use of advanced photon-processing semiconductor X-ray detectors with optimum sensor materials. This study addresses the investigation of the optimum semiconductor sensor material for mammography in combination with the photon-processing detector Medipix3RX. The influence of K-shell fluorescence from the sensor material on the achievable contrast-to-noise ratio is investigated, as well as the attenuation efficiency. The three different sensor materials, CdTe, GaAs, and Si are studied, showing advances of CdTe-sensors for mammography. Furthermore, a comparison of the contrast-to-noise ratio between a clinical Se-detector and Medipix3RX detectors with Si- and CdTe-sensors is shown using a self-produced mammography phantom that is based on real human tissue.**

***Index Terms*— CdTe, contrast-to-noise ratio, GaAs, human phantom, mammography, Medipix3RX, spatial resolution, X-ray attenuation efficiency.**

I. Introduction

THE benefits of mammography screening have been controversially discussed for years. Despite the number of studies that show that detection of tumors at an early stage, by the use of mammography evaluation, increases the survival rate of patients, the radiation exposure itself leads to the statistical fact that a small fraction of women may develop breast cancer as a direct result of X-ray mammography screening [1], [2].

As of 2019, about 40 million annual mammography procedures are reported only in the U.S. [3]. The mean organ dose per digital mammography exam per person is 5.3 mGy (1.33 mGy per exposure, four exposures usually performed [4]–[6]). Some studies estimate a lifetime attributable risk (LAR) of radiation-induced fatal breast cancer associated with annual digital screening or screen-film mammography of 20-25 cases per 100,000 in women aged 40-80 years [5]. By decreasing the dose in mammography, the number of examination-induced collateral effects could be significantly reduced. Therefore, a further reduction of the mortality of women by the use of mammography could be achievable [7], [8].

As shown by McCullagh *et al.* [9] the usage of photon counting detectors reduces the organ dose by typically 46 %, even though the photon-counting detector (Sectra MDM L30) used for their studies is based on a Si-sensor, which does not provide optimum X-ray absorption efficiency. A photon counting detector combined with a high-Z sensor material, with near 100 % absorption efficiency for the X-ray energies used in mammographic examinations, could achieve a remarkable organ dose saving for mammography.

Considering that early diagnosis of cancer lesions is beneficial for successful treatment, the need to detect lesions and microcalcifications in their earliest possible formation phase motivates for diagnostic imaging with high spatial resolution [10]. A higher spatial resolution increases image sharpness and allows for better recognition of low contrast pathological lesions and of morphological characteristics of microcalcifications during image analysis. Thus, spatial resolution of X-ray detectors used for mammography is an important property.

Current clinical mammography systems have detectors with a pixel pitch between 50 μm and 100 μm [11]. A pixel pitch of 50 μm corresponds to a Nyquist spatial frequency of 10 line-pairs per mm (lp/mm) allowing for aliasing-free detection of objects with size $\geq$ 100 μm. As for mammography the desired aliasing-free object detection resolution is 50 μm [12], geometrical magnification and electronic data processing of the detector signal is being used to achieve a high spatial resolution.

Despite these efforts, the detection of small low contrast structures is challenging, because all clinically used detectors

Manuscript received February 11, 2020; revised April 24, 2020 and June 9, 2020; accepted June 21, 2020. Date of publication June 24, 2020; date of current version November 30, 2020. This work was supported in part by the German Ministry of Research and Education (BMBF) through the MAMMOSECUR Förderkennzeichen Project under Grant 01DN19002, in part by the Colombian Ministry of Science, Technology and Innovation (COLCIENCIAS) Project under Grant 80740-055-2019, and in part by the Faculty of Science, Universidad de los Andes, under Project P18.160322.001-15FISI01. *(Corresponding author: Simon Procz.)*

Simon Procz and Michael Fiederle are with the Freiburg Materials Research Center, Albert-Ludwigs-Universität Freiburg, 79085 Freiburg im Breisgau, Germany (e-mail: simon.procz@fmf.uni-freiburg.de; michael.fiederle@fmf.uni-freiburg.de).

Gerardo Roque, Carlos Avila, and Jorge Racedo are with the Department of Physics, Universidad de los Andes, Bogotá 111711, Colombia (e-mail: ga.roque10@uniandes.edu.co; cavila@uniandes.edu.co; jm.racedo235@uniandes.edu.co).

Roberto Rueda is with the School of Medicine, Universidad de los Andes, Bogotá 111711, Colombia (e-mail: rj.rueda32@uniandes.edu.co).

Ivan Santos is with the Department of Plastic Surgery, Fundación Santa Fe de Bogotá University Hospital, Bogotá 110111, Colombia (e-mail: paciente@ivansantos.com).

Color versions of one or more of the figures in this article are available online at https://ieeexplore.ieee.org.

Digital Object Identifier 10.1109/TMI.2020.3004648

have a modulation transfer function (MTF) contrast below 30 % at high spatial frequencies of 10 lp/mm [13]. For photon counting X-ray detectors, such as the Medipix3RX, it has been shown that they achieve a significantly higher MTF-contrast than any other currently used clinical X-ray detector [14], [15]. Therefore, such detectors are able to improve the detection of small structures.

Regardless of the potential improvements that photon counting detectors could provide for mammography, the research to implement these detectors in clinical X-ray breast screening declined in the last decade. A reason for this is the size of the photon counting sensors; they offer typically a limited area, which is not sufficient for mammography detectors, which demand large areas of minimum 17 × 23 cm^2, and ideally 24 × 30 cm^2. Due to recent progress in Through-Silicon via (TSV) connection technology [16] and seamless large area tiling technology [17], it is technically possible to build such a large sensitive area photon counting detector now. This makes the utilization of photon counting detectors for mammography feasible.

In this paper, the performance of a Medipix3RX detector-based imaging system for mammography is evaluated. The first part of this document deals with the influence of different sensor materials like Si, GaAs, CdTe, and Se in mammography imaging. The second part covers the comparison of a clinical mammography system with a CdTe-Medipix3RX imaging setup using a human breast tissue phantom.

II. Materials and Methods

A. Detectors and Sensors

The clinical mammography system "Hologic Selenia Dimensions w/AWS 5000" used in this study is based on a thin film transistor flat panel detector with an amorphous Selenium (a-Se) sensor [18]. The a-Se sensor converts X-ray photons directly into charges and the signal intensity is a measure of the total integrated charge per pixel. The detector has a pixel pitch of 70 μm, a total active area of 24 × 29 cm^2 with 3328 × 4096 pixels and an a-Se thickness of 200 μm [18]–[20]. The usual sensor bias voltage is 10 kV [21].

The photon counting semiconductor detectors used in this study are mainly based on the Medipix3RX ASIC [22] bump bonded to CdTe-, GaAs- and Si-sensors. The Medipix3RX detector is under continued development by the "Medipix3 Collaboration" at CERN [23] and has 256 × 256 pixels with a pixel pitch of 55 μm. The pixel pitch of the Medipix detector ASICs is the smallest of all photon-counting detector ASICs [24], therefore making the Medipix3RX a reasonable candidate for investigations on high-resolution mammography detectors. The Medipix3RX features up to eight adjustable energy thresholds with individual counters allowing multispectral X-ray imaging and two different operation modes: The so-called Single Pixel Mode (SPM), which operates every pixel individually, and a mode with correction for charge sharing, the Charge Summing Mode (CSM).

For dose calibration, a Timepix1 [25] detector with 300 μm Si-sensor was employed. The Timepix1 detector features the same pixel pitch and size as the Medipix3RX detector, but instead of using multiple thresholds and counters, it offers the so-called Time-over-Threshold (ToT) mode. This mode gives spectroscopic information about the energy of each registered X-ray photon.

TABLE I
A Sensors Assembled for Material Comparative Study
B Sensors Assembled for Comparative Study With Commercial Setup

(a)

Sensor Material	Material Thickness	Material Information
CdTe	450 µm	"Acrorad" CdTe material [16] / FMF processing.
GaAs	500 µm	Cr-compensated "Tomsk" GaAs material [17] / FMF processing.
Si	500 µm	Standard p^+n silicon detector.
Si	300 µm	Standard p^+n silicon detector.

(b)

Sensor Material	Material Thickness	Material Information
CdTe	1 mm	"Acrorad" CdTe material / FMF processing.
CdTe	3 mm	"Acrorad" CdTe material / "Acrorad" processing.

All Medipix and Timepix chips are three-side buttable allowing the assembly of detector line modules with monolithic sensors up to 2 × 8 chips [26], or almost seamless large area detectors with single edgeless sensors up to presently 10 × 10 chips [17].

Currently, the four sensor materials CdTe, CdZnTe, GaAs, and Si can be assembled to photon counting readout chips, which operate at room temperature without active cooling. For the comparison of these sensor materials, thin sensors have been processed, as can be seen in Table 1A. CdZnTe was not available for this study and it is therefore not included here, but as shown by Barber *et al.* [27] it should perform similar to CdTe in this energy range, as the content of Zn in CdZnTe is low with typically about 10 % [28]. For comparison between the clinical Hologic Selenia mammography system and the Medipix3RX system, two more detectors were fabricated, as can be seen in Table 1B. An a-Se based sensor as the one used in the Hologic system cannot be implemented with photon counting Medipix detectors due to the very low mobility of charge carriers in a-Se [29], which prohibits the use of this sensor material with non-charge-integrating detectors.

All Medipix3RX and Timepix1 detectors have been operated in standard photon counting mode SPM. For CdTe- and GaAs-sensors, a negative bias voltage was applied to the common electrode of the detector, whereas for the standard Si p+n sensor, a positive bias voltage was supplied. The output of the Charge Sensitive Amplifier (CSA) in the pixel electronics reflects the movement of charge carriers in the sensor due to the bias voltage. The detectors were equalized by count rate equalization [30], which is a good compromise between equalization effort and spectral uniformity. It gives a better result than standard equalization with the electronics noise floor. The threshold energy calibrations were performed by the

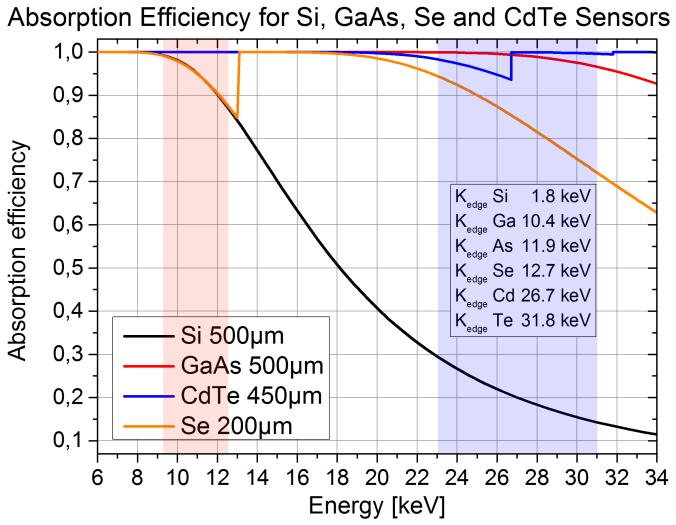

Fig. 1. Comparison of absorption efficiency of Si, GaAs, a-Se and CdTe sensors with thicknesses as used in this study, including the K-shell X-ray fluorescence energies of GaAs, Se and CdTe. The GaAs and Se fluorescences with an energy of 9.2-12.5 keV are well within the spectrum used for mammography and thus affecting the measurement. Contrary to this, the CdTe fluorescences with an energy of 23.1-31.1 keV are at the border of the mammography spectrum and do not influence the measurement significantly, especially because only a small fraction of the mammography spectrum is higher than the K-edge of Cd at 26.7 keV. The attenuation efficiency at 22-27 keV is slightly higher for GaAs than for CdTe due to the K-edge of Cd. The K-edges of Ga and As are not visible as a 500 μm thick GaAs-sensor has a complete X-ray absorption at these energies. Si does not have a K-fluorescence in the mammographic energy range, but the attenuation efficiency is not optimal for mammography.

use of the K_α fluorescence of different metals [30]. The low threshold (E_{min}) of all Medipix3RX and Timepix1 detectors was set to the same value of 5.0 ± 0.2 keV for all contrast and dose measurements. Such a low energy threshold was used to minimize event losses caused by charge sharing and fluorescence. All photons above this energy have been counted, a high threshold (E_{max}) was not used. For all detectors, this threshold was above the electronics noise floor, therefore electronic noise was discriminated and not significantly contributing to the signal.

All acquired images have been corrected by flatfield [31]. A beam hardening correction [32] was performed as well, but the results were worse than those obtained by a standard flatfield correction due to the long-term counting behavior changes in the sensors, therefore a flatfield correction was used in this work.

In contrast to common radiologic imaging, all radiographs presented in this paper use a proportional scaling of X-ray intensity values, which means that objects with high attenuation are black, whereas objects with low attenuation are white. Figure 1 shows a comparison of the X-ray absorption efficiency, within the photon energy range for mammography applications, for Si-, GaAs-, Se- and CdTe-sensors used in this study.

B. Mammography Phantoms

Two different mammography phantoms were employed in this study. For assessment of different sensor materials with Medipix3RX detectors, a commercial phantom was used. For the comparison between a clinical system and Medipix3RX detectors with CdTe- and Si-sensors a new phantom, based on real human breast tissue, was designed and built.

1) Commercial Mammography Phantom: The commercial mammography phantom TOR MAM (Leeds Test Objects Ltd, North Yorkshire, United Kingdom [33]) was adopted in this study for the investigation of the suitability of different sensor materials for mammography. The commercial phantom consists of two parts: the right part emulates the female breast tissue for use in clinical routine; the left part features different test structures, including microcalcifications and low-contrast discs simulating tumorous tissue. These low-contrast test objects were considered in our study for the assessment of different sensor materials. A photograph of the commercial phantom is shown in Fig. 2, as well as the radiography of it, using a CdTe-Medipix3RX detector with 450 μm sensor thickness, and a tiling method for acquisition of the full phantom.

2) Human Breast Tissue Phantom: This study addresses the simulation of all conditions found in real mammography imaging, going one step further by assembling a human-tissue mammographic phantom. The phantom is built from human breast and fat tissues extracted from breast-reduction and cosmetic abdominoplasty patients, who gave their written au-thorization for the use of their extracted tissues in the present study. One single phantom prototype was constructed. Sample manipulation, transportation, and other technical and logistic considerations were assessed to follow clinical standards.

The morphology of the phantom was designed to mimic the histological and anatomical configuration of a human breast, adding a thinner adipose tissue layer, below which breast tissue portions were stitched to achieve the desired thickness. The geometry was adjusted to emulate a standard compressed breast of 4.0 cm thickness.

All the construction process was designed to achieve a phantom with X-ray absorption properties and morphology similar to a real breast. As a final step, Calcium Hydroxyapatite (HA) amorphous crystals, ranging in sizes from 120 μm up to 500 μm, were used to simulate the gestating cancer tissue. All the crystals were placed in the middle of the phantom, in between the two different tissue types. The crystals were assembled in three different planar geometric distributions, as indicated in Fig. 3c. For the present study, the focus is on a 5×5 matrix distribution with rows of crystals of about same size, with varying sizes from one row to the next (phantom section 2).

A particular issue arose from the continued manipulation of the phantom, requiring special care for tissue and morphology preservation over time. In many cases, work with biological tissue and some radiological phantoms require refrigeration [34]. In this study, the preservation temperature for the phantom was fixed at -20 °C and transportation was carried out by using a thermally isolated container with frozen gel inside. Freezing has the added benefit of fixing the structure of the phantom, and thus allowing for repeatability of measurement, for as long as the phantom is frozen. Once the phantom

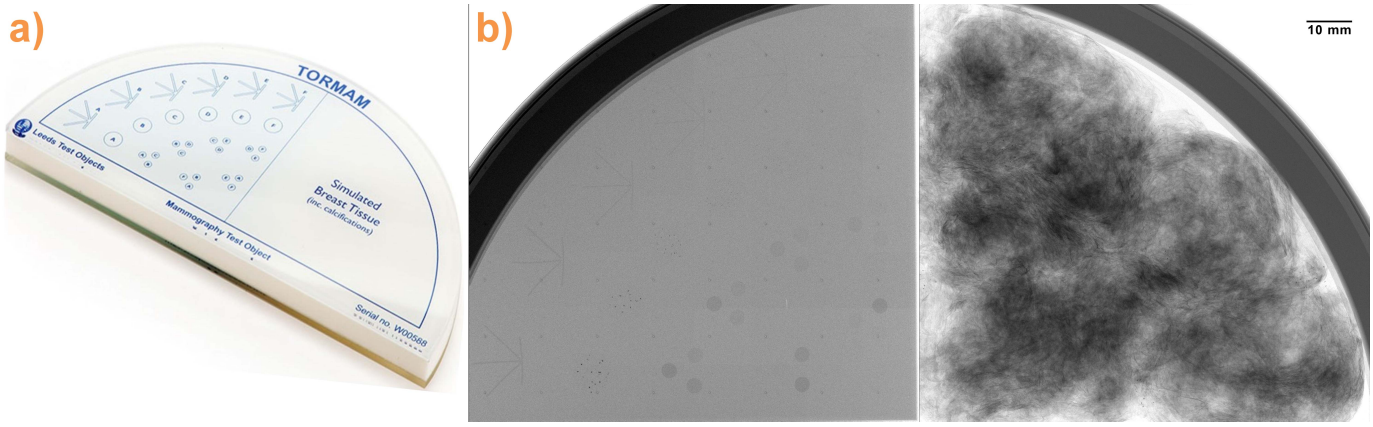

Fig. 2. a) Commercial mammography phantom photography and b) radiographic examination, acquired with 16 × 8 tiling with a Medipix3RX detector with a 450 μm thick CdTe-sensor with 55 μm pixel pitch. A bias voltage of −230 V, a low threshold of 5 keV and the Single Pixel Mode were used. The left part of the phantom features different test structures, including microcalcifications and low-contrast circles simulating tumorous tissue. The right part simulates a human female breast. The left part of this phantom was used for sensor material comparison.

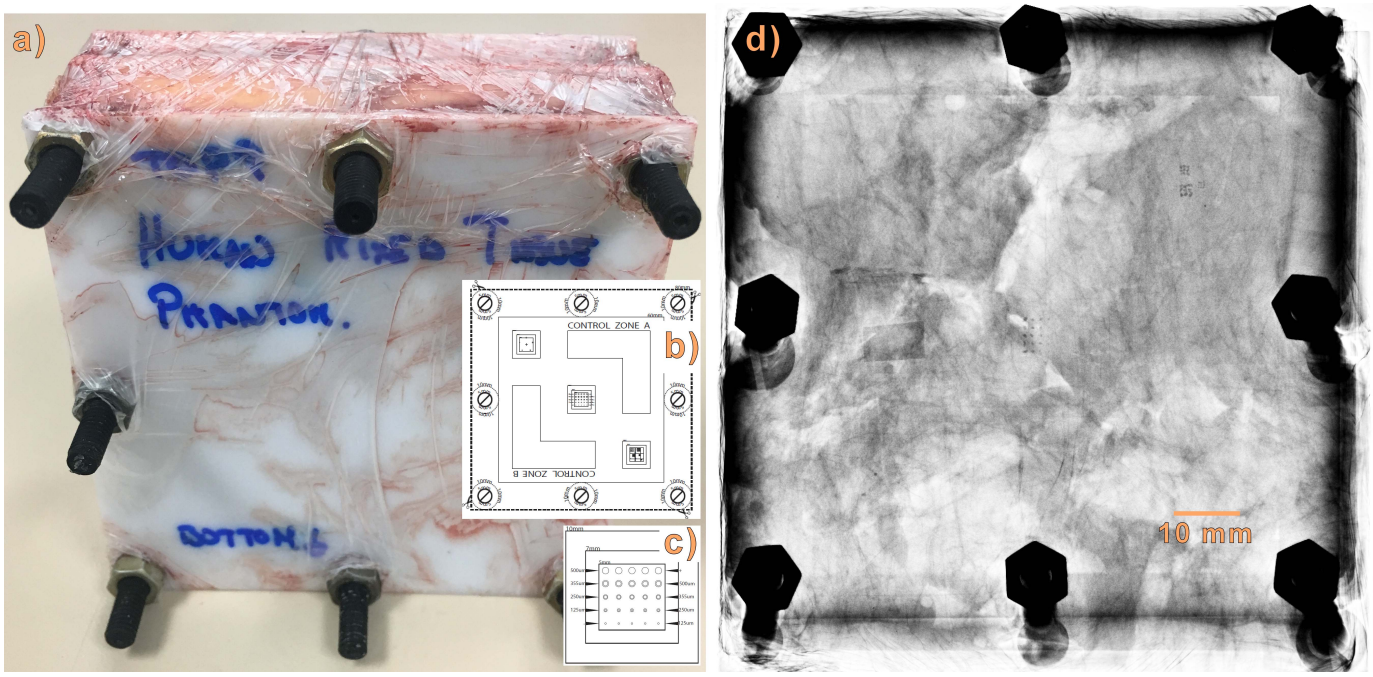

Fig. 3. a) Photography of the human tissue mammography phantom that was designed and constructed for this study, including a drawing b) of the different sections and a detailed view c) of the central section. Figure d) shows a full-size radiography of this phantom, acquired with the Hologic Selenia system. The central section pattern is visible in the center.

stabilizes thermally with the environment, melting from the water and tissue fluids displaces the internal structure. Even though this was initially accounted for, via stitching and frame construction, the weight of the tissue itself, once unfrozen, is enough to cause a noticeable displacement. This effect is particularly noticeable at the experimental laboratory setup due to two reasons. First, the geometry of the setup itself. The sample is standing up, in front of the detector in a horizontal configuration, different to the commercial setup, where the sample is laying on top of the detector in a vertical configuration. Second, the time needed for data acquisition is different between the two systems evaluated. Because of the lower power of the laboratory X-ray source, the acquisition time is up to two orders of magnitude higher than for the clinical setup.

C. Experimental Setup

Comparisons are carried out between two different setups. The first setup is the Hologic Selenia Dimensions. Acquisitions with this system were performed in a clinical mammographic facility. This system is equipped with an X-ray tube with a W-anode, an Rh-filter of 50 μm in thickness and a further 3 mm PMMA filter (breast holder). The X-ray beam spot size is 100 μm. The detector used is an a-Se flat-panel TFT as described in section II-A. The source-to-detector distance was 70.0 cm, and the source-to-object distance 61.6 cm. For all measurements, the X-ray source was set to 28 kVp, while the tube current was changed from 40 mAs, which is the lowest stable value that could be set for this system, up to 90 mAs, which was the standard value for the radiation dose calculated by the system for the used phantom.

The second setup is a self-made laboratory X-ray imaging system [35], [36], which is equipped with a low-power microfocus Hamamatsu L10321 X-ray source with a W-anode, an Rh-filter of 50 μm thickness and a 3 mm PMMA filter. A scattering shield was applied at the X-ray tube window. The X-ray beam spot size for this system is 5 μm. For all measurements, the X-ray source was set to 28 kVp, the same as for the Hologic Selenia system. The tube current was constant at 150 μA, and the detector acquisitions were split into multiple short-time measurements to achieve results with different doses. Various Medipix3RX based detectors have been used here, as described above. The source-to-detector distance was 70.0 cm, and the source-to-object distance 61.6 cm, in order to achieve the same magnification of 1.13× as with the clinical system.

D. Dose Calibration

As the clinical system was in routine use, it was not available for long-lasting measurement series with Medipix3RX detectors. As one topic of this paper is the comparison of the results of two different detectors, knowledge of the radiation dose is necessary. For this reason, a series of measurements using a Timepix1 detector with a 300 μm thick Si-sensor has been performed to calibrate the dose. A Timepix1 detector was chosen here instead of a Medipix3RX detector because of the higher maximum frame rate with the available readout [37].

As both systems use exactly the same kind of X-ray spectrum and magnification, the dose can be directly compared by calculation of the X-ray flux. For this purpose, the Timepix1 detector was placed at the position of the mammography phantom. The acquisition time was set to a low value of 0.5 μs, so that registered photons could be counted individually without a significant fraction of event pileup. The detector was acquiring continuously during the time the mammographic measurement with the Hologic system was performed. This was done for the standard dose setting (90 mAs) and the lowest possible setting (40 mAs). It was found, that the pulse of the X-ray source has a rectangular shape with a length of 0.420 $\pm$ 0.019 seconds and a mean of 1398 $\pm$ 73 photon counts per frame for the 40 mAs setting, respectively a length of 0.88 $\pm$ 0.04 seconds and a mean of 1512 $\pm$ 70 photon counts for the 90 mAs setting.

As very short Timepix1 acquisition times, like 0.5 μs, are outside of the detector's linear range, the real acquisition times have been studied in the laboratory setup. A measurement series with different set acquisition times from 0.5 μs until 2000 μs was performed to calculate the corresponding real acquisition times. For the set value of 0.5 μs, the measured real counting time was found to be 2.5 μs.

To achieve the same mean count value of 1398 counts per frame for the laboratory X-ray source, the acquisition time had to be 1.23 ms, and 1.34 ms for the 1512 counts measurement, respectively. With these measurements, the equivalent exposure times for the lab source were calculated to 205.8 s (corresponding to 40 mAs of the Hologic Selenia system with 0.42 s exposure time), and 467.4 s corresponding to the 90 mAs measurement equivalent. For verification, all dose calibration measurements and calculations have been additionally performed with 5 μs time setting for the Timepix1 detector. The deviation between these two calibration measurements was 0.3 % and thus within the statistical error tolerance.

III. Results and Discussion

A. Influence of Sensor Material Fluorescence on Image Quality

As shown in Fig. 1, the attenuation efficiencies of GaAs, CdTe and Se are very high for the energies used in mammography, even for thin sensors, whereas Si is less efficient. If Si is used as sensor material, much thicker sensors are necessary to achieve acceptable detection efficiency for mammography. For a typical mammography spectrum (Rh-filtered, W-anode, 30 kVp) peaking at 23.2 keV, a thickness of 6.6 mm is required for Si-sensors to achieve 99 % efficiency, whereas for GaAs 230 μm and CdTe 500 μm are sufficient for obtaining the same stopping power. As charge sharing effects arise with increasing sensor thickness [38], a lower contrast and image sharpness is achieved by detectors with thick Si-sensors.

Despite the higher mass attenuation efficiency of GaAs in the mammography energy range, CdTe-based sensors still show a better image quality if all registered photons are detected. The reason for this is the X-ray fluorescence of the used sensor materials. Whereas GaAs is generating fluorescence mainly in the range of 10-12 keV, the energy for CdTe fluorescence is significantly higher, in the range 27-33 keV. In the typical mammography energy range, between 26-32 kVp [39], [40], most of the X-ray flux is directly above the K-edge of Ga and As, and therefore able to generate X-ray fluorescence with high yield [41]. For CdTe, only a very small proportion of the incident spectrum can generate X-ray fluorescence. The effect of fluorescence on image contrast and sharpness is shown in Fig. 4. The CdTe-sensor with 450 μm thickness in Fig. 4c can reproduce a line-pair pattern with a high contrast up to the Nyquist limit of the detector chip of 9.1 lp/mm without increasing the detector threshold. For a mean contrast fraction of 0.5 between the line pairs, a value of 9.5 $\pm$ 0.3 lp/mm was measured for 7.5 keV threshold.

For GaAs the situation is different: if the detector threshold is set to a low value of 7.5 keV, so that a high percentage of incoming events is registered, then image contrast and sharpness significantly drop, as shown in Fig. 4a. Here, the line-pair pattern is distinguishable only up to 5.3 $\pm$ 0.6 lp/mm. If the detector threshold is increased to 13 keV, above the fluorescence energy of GaAs, then the image contrast and sharpness improve as shown in Fig. 4b, up to 8.8 $\pm$ 0.4 lp/mm. This improvement in spatial resolution comes at the price of a significantly decreased detection efficiency, which drops to 36% of the efficiency at 7.5 keV threshold. The spatial resolution of the 500 μm thick Si-sensor is not shown in Fig. 4, as it is very similar to Fig. 4b and Fig. 4c. The measured resolution was 9.0 $\pm$ 0.3 lp/mm. These spatial resolution measurements are in good agreement with published values [42]–[44].

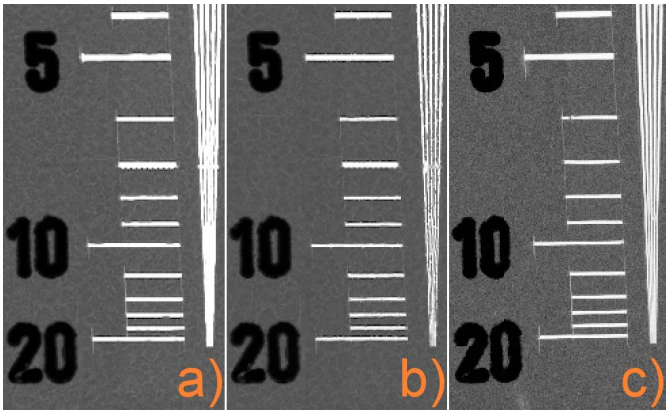

Fig. 4. Influence of sensor fluorescence on image sharpness using a line pattern resolution test object. a) 500 μm GaAs, 7.5 keV detector threshold. b) 500 μm GaAs, 13 keV threshold. c) 450 μm CdTe, 7.5 keV threshold. Due to fluorescence of Ga and As, image sharpness is severely decreased if the detector threshold is set to a value such that all incoming photons are being registered. If the threshold value is set above fluorescence energy, as in b), contrast and resolution improve. Image sharpness of CdTe c) is high already for 7.5 keV threshold as the fluorescence is negligible.

B. Sensor Comparison With Medipix Detectors

Two measurement approaches have been performed to evaluate the performance of the Medipix3RX detector chip for mammography with different sensor configurations. The first measurement series uses different sensor materials with a similar thickness to investigate their influence. The second measurement series uses CdTe-sensors with different thicknesses to evaluate the optimal sensor for a comparison with a clinical system. Both measurement series use the standard photon counting mode (SPM) of Medipix3RX with a low energy threshold of 5.0 ± 0.2 keV as described in section II-A. The X-ray spectrum was set to 28 kVp with 50 μm Rh-filtering.

1) Evaluation of Different Sensor Materials: For comparison of the sensor materials Si, GaAs, and CdTe, bump bonded to Medipix3RX readout chips, a measurement series with the commercial phantom was performed in the laboratory setup. Thin semiconductor sensors have been processed for this purpose with a thickness of 500 μm for Si and GaAs, and 450 μm for CdTe. For all detectors, the count rate as a function of the bias voltage was measured, and the optimum bias voltage was determined as the value where count rates plateau. For the 450 μm CdTe-sensor, the bias voltage was -230 V with a high leakage current of 80 μA, which is explained in the next section. For the GaAs-sensor, the bias voltage was -240 V and leakage current of 12 μA. For the Si-sensor, the bias voltage was $+140$ V with a leakage current less than 1 μA. The leakage current of the sensors was measured, after detector assembly, by monitoring the total DC current consumed by the sensors from the high voltage supply over the common electrode. The detector was running at measurement conditions and ready for imaging, but without X-ray flux, to achieve thermal equilibrium.

For each detector, two measurements have been performed with two different entrance doses: 4.3 mGy as a typical mammography entrance surface dose (ESD), and 0.43 mGy, corresponding to 10 % of the typical dose. The contrast-to-noise ratio (CNR) was calculated for the low-contrast test structure shown in Fig. 5, by using eq. (1).

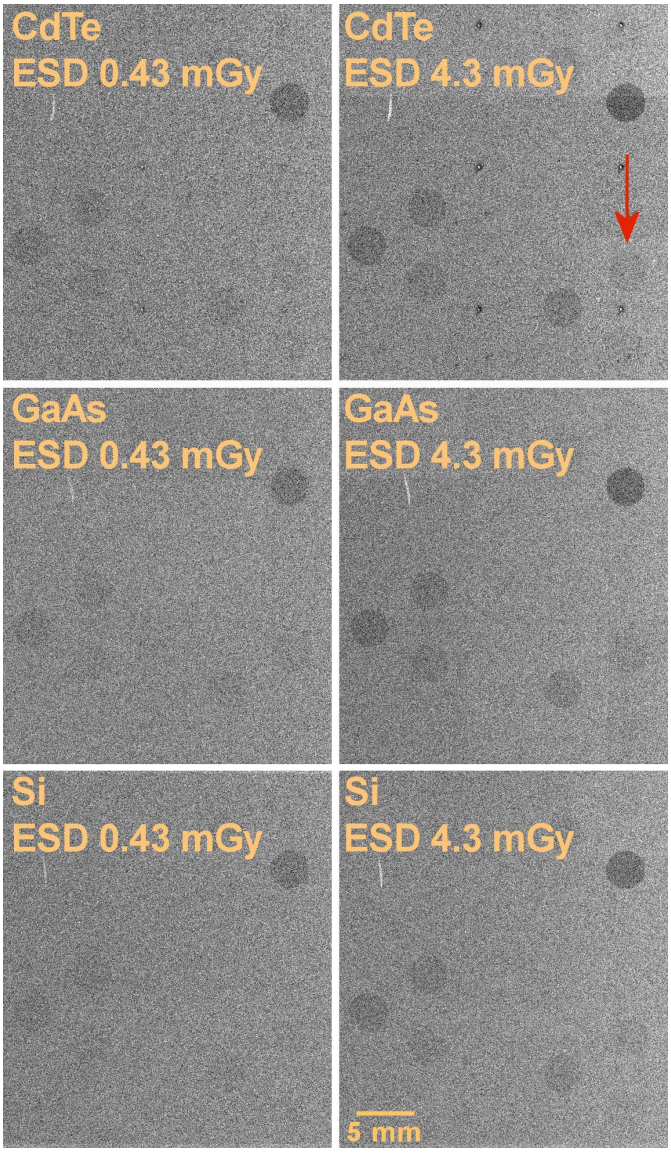

Fig. 5. Contrast comparison of the commercial phantom with CdTe-, GaAs- and Si-sensors for two different ESD values. The low contrast structure that was used for CNR calculations is indicated with an arrow.

$$CNR = \frac{\left|S_{background} - S_{object}\right|}{\sigma_{background}} \tag{1}$$

Here, $S_{background}$ stands for the signal in the background, S_{object} for the signal in the object of interest, and $\sigma_{background}$ for the noise of the background. This test structure represents a 3 mm small tumor with low contrast to surrounding tissue. For calculation of the CNR, the tumor-like circle area was used as object (2561 pixels), as indicated by an arrow in Fig. 5. For the background, a homogenous area (3313 pixels) was used. The calculated CNR values are shown in Table II.

The best CNR was achieved with the CdTe-sensor. For the standard entrance dose value of 4.3 mGy, a CNR of 0.50 was determined. This value is significantly higher than for the GaAs-sensor, which results in 0.43, and reduces to 0.31 if the

TABLE II
MEASURED CNR VALUES FOR THIN SENSOR MATERIALS

Sensor Material	CNR ESD = 0.43 ± 0.02 mGy	CNR ESD = 4.30 ± 0.13 mGy
CdTe	0.30	0.50
GaAs	0.31 (0.22[a])	0.43 (0.31[a])
Si	0.13	0.31

Measurements of contrast-to-noise values with thin sensors at a low contrast structure of the commercial phantom for two different ESD values.
[a] Values for GaAs-detector, measured with an increased threshold, from 7.5 keV to 13 keV to achieve the same spatial resolution as with the CdTe-sensor.

detector threshold is raised to 13 keV to maintain the spatial resolution. For the Si-sensor, the value of 0.31 is the lowest and comparable with the CdTe value of 0.30, that was already achieved with 10 % of the standard dose. For GaAs, a similar value of 0.31 was found for the low dose measurement, but this value drops to 0.22 if the detector threshold is raised to 13 keV. Due to the low attenuation efficiency, the Si-sensor provides a CNR of only 0.13 for the 0.43 mGy entrance dose measurement, which is less than half of the values achieved with CdTe and GaAs.

The main reason for the higher CNR of the CdTe sensor, in comparison to the GaAs sensor, is the significantly lower amount of X-ray fluorescence photons being emitted from Cd and Te than from Ga and As as described in section III-A and Fig. 1. The higher CNR with CdTe was achieved despite the 2.5 times higher leakage current of this sensor, with respect to the GaAs sensor.

Given these results, CdTe was chosen as the sensor material for further comparison with a clinical Se-sensor based system. In order to get the best results, different CdTe-sensors have been compared first.

2) Comparison of Different CdTe-Sensors: The processing of CdTe is still an elaborate, manual process and the optimization of processing parameters is an ongoing research development. Three CdTe-detectors with different thicknesses have been manufactured and characterized for their suitability for mammography. The thickness of the CdTe-sensors were 450 μm, 1 mm and 3 mm. Whereas the 1 mm and 3 mm CdTe-sensors have been processed at wafer-level, the 450 μm sensor was thinned and reprocessed after dicing. For all detectors, the count rate as function of the bias voltage was measured the same way as in the previous section. For the 450 μm thick sensor, the bias voltage was −230 V with a leakage current of 80 μA. Due to the fragility of the thin CdTe material, the edges of this 450 μm thick sensor have been non-smooth causing very high surface leakage currents. Dicing can produce several defects on the crystal edges, degrading charge transport and therefore increasing the surface leakage currents [45], [46]. Furthermore, imperfections during chemical surface treatment, contact processing and bump bonding are contributing factors for the high leakage current of this sensor. This is also evident for the 1 mm thick sensor, where the bias voltage was −320 V with 30 μA leakage current, which is still more than a magnitude higher than the bulk value due to high surface leakage currents caused by imperfect sensor edges, bump bonding and contact processing. For the 3 mm sensor new contact processing and dicing methods and tools were used, resulting in significantly lower leakage currents. For this case, the leakage current was 10 μA at −1200 V bias voltage.

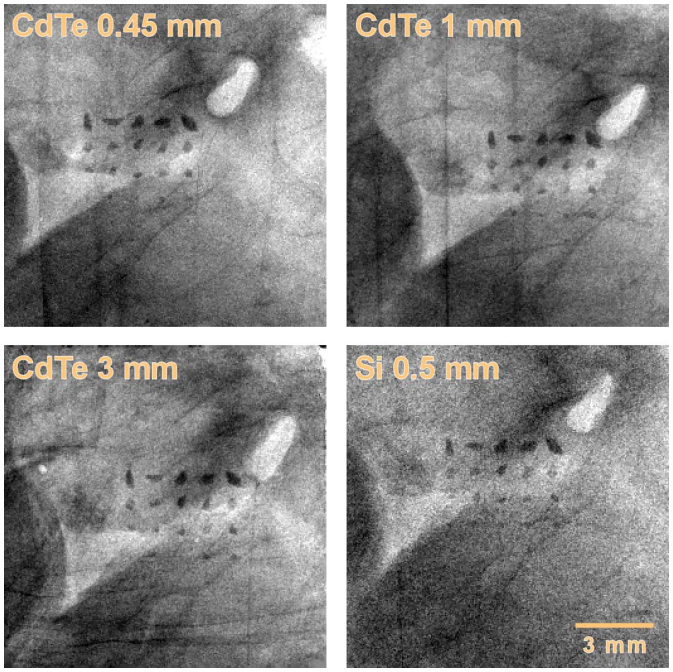

Fig. 6. Comparison of X-ray images of section 2 of the human tissue mammography phantom. The spatial resolution is similar for all sensors, but highest for the 1 mm CdTe-detector. The noise for the Si-sensor is visibly higher due to the low attenuation efficiency of Si. The calculated CNR of the 1 mm thick CdTe-sensor is higher than for the 450 μm thick sensor because of a significantly lower leakage current.

Fig. 6 shows section 2 of the human breast tissue phantom, acquired with these three CdTe-detectors and additionally a 300 μm thick Si-detector as a reference. These images are flatfield corrected and have a nearest-neighbor interpolation for dead pixels. The ESD was set to a value of 3.9 ± 0.1 mGy for all measurements, corresponding to an average grandular dose (AGD) of 0.95 ± 0.12 mGy.

For assessment of the best CdTe-detector, charge sharing was measured and the CNR of HA-crystals was calculated. Charge sharing depends on the sensor material, sensor thickness, bias voltage, pixel size and incoming photon energy [47], and it affects negatively the image sharpness [48]. For quantitative determination of charge sharing, the Medipix3RX detector acquisition time was reduced to such an extent that only individual events were registered. Then the cluster size of 10,000 frames was analyzed for each detector. The mean cluster sizes and the corresponding standard deviations are shown in table III. As expected, the amount of charge sharing is increasing with detector thickness. For calculation of the CNR, the smallest visible HA-crystals with 125 - 250 μm diameter average size were selected as the region of interest (ROI). For the ROI, only crystals were selected (47 pixels), without surrounding back-ground. For the background, a homogenous white tissue area was selected (189 pixels). Besides the nearest-neighbor interpolation for dead pixels, no image processing was performed.

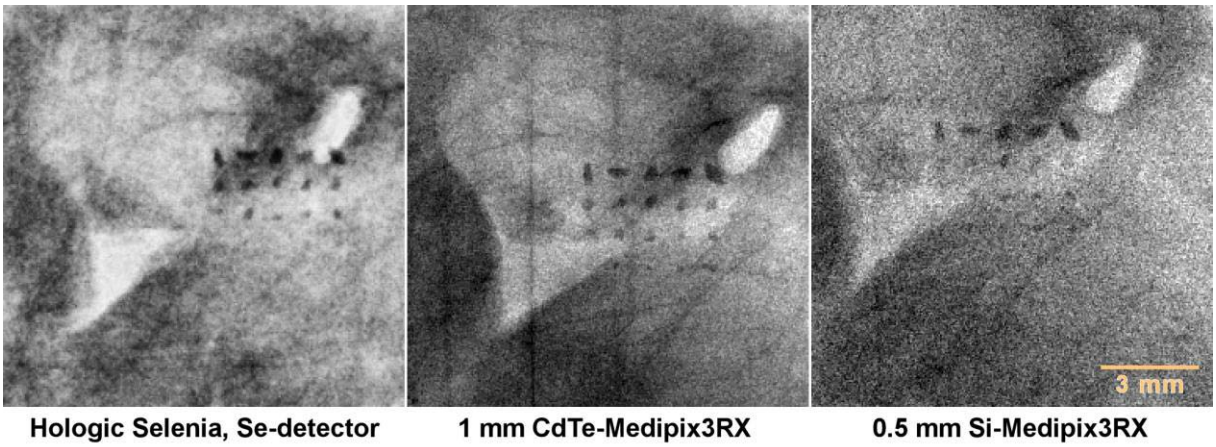

Fig. 7. Comparison of section 2 of the human breast tissue phantom between Hologic Selenia Se-detector, CdTe-Medipix3RX and Si-Medipix3RX. The dose was reduced by 55 % compared to the standard dose. The image quality of the CdTe-Medipix3RX is superior to the other detectors in terms of spatial resolution, contrast and noise.

TABLE III
MEAN CLUSTER SIZES AND CNR VALUES FOR CdTe EVALUATION

Sensor	Cluster Size: mean ± SD [pixel]	CNR
CdTe 450 µm	1.39 ± 0.51	9.7
CdTe 1 mm	1.66 ± 0.60	15.2
CdTe 3 mm	2.07 ± 0.73	11.2
Si 500 µm	1.38 ± 0.48	7.1

Mean cluster sizes and CNR values of the 4th HA-crystals row.

Despite the higher thickness and therefore higher charge sharing of the 1 mm sensor, compared to the 450 μm thick sensor, the image result is better because of the lower leakage current. The higher the leakage current of a CdTe-sensor is, the faster the sensor changes its counting behavior [49], especially in areas like dislocation networks and backside damages. The high leakage current of the 450 μm detector negatively influences the image quality. For the 3 mm detector the leakage current is even lower than for the 1 mm case, but because of the higher detector thickness charge sharing is more pronounced, the image sharpness is slightly softer in comparison to the 1 mm detector, along with a decrease in the CNR of small HA-crystals. The image quality of the Si-detector is worse than for CdTe-sensors because of the lower attenuation efficiency of the Si-sensor and hence a higher noise level.

For these reasons, the 1 mm thick detector was chosen for comparison with the Hologic Selenia system.

C. Comparison of a CdTe-Medipix3RX With a Clinical Selenia System Using a Human Breast Tissue Mammography Phantom

The comparison between the clinical mammography detector of the Hologic Selenia system and a Medipix3RX based detector with CdTe- and Si-sensors was performed at two different setups. The reason is the routine use of the clinical system, which prevents direct comparison with the same X-ray system due to the long lasting pre-calibration measurements for the Medipix3RX detectors for this study. Therefore, the Medipix3RX measurements have been obtained in a laboratory setup with comparable conditions to the clinical setup, as described in section II-C.

For the clinical system, in total six radiographs were acquired with X-ray tube currents setting from 40 mAs to 90 mAs, in 10 mAs increments. These values correspond to ESD ranging from 1.76 ± 0.05 mGy to 3.9 ± 0.1 mGy, which are typical mammography dose values.

The Medipix3RX measurements were performed sequentially summing up single acquisition frames. In this way, dose-dependent results in small 1 % steps from 1 % to 160 % of the standard dose of the clinical system have been obtained. Before the actual measurements, frames were pre-acquired with the Medipix3RX detectors for 30 min to achieve thermal stability of the sensor.

Fig. 7 shows the comparison of section 2 of the human breast tissue phantom between the Se-detector of the Hologic Selenia system and the Medipix3RX detectors with 1 mm thick CdTe- and 500 μm Si-sensors, at a significantly reduced dose. The ESD was 1.76 ± 0.05 mGy, which corresponds to a reduction of 55 % compared to the standard dose. The image resolution of the Medipix3RX with CdTe-sensor is superior to the other detectors. The structure of the tissue is visible whereas the Se-detector shows a notable blurring, and the Si-detector has a strong noise because of the low counting statistics due to its low attenuation efficiency. The fourth HA-crystal row with crystal sizes between 125 μm and 250 μm is visible with both Medipix3RX detectors, but not evident with the Se-detector. From the fifth HA-crystal row with crystal diameters less than 125 μm, two crystals are recognizable with the CdTe-Medipix3RX, but none with the other detectors. The a-Se-detector shows a visible pattern in a grid of six pixels, which makes identification of very small structures more difficult.

Fig. 8 compares the mammography results of the Se-detector with the CdTe-Medipix3RX. As the pixel sizes of both detectors are different, 70 μm vs. 55 μm respectively, the pixels were multiplied by a factor of 4 for the CdTe-Medipix3RX and a factor of 5 for the Se-detector. This way a direct comparison of the images is possible without

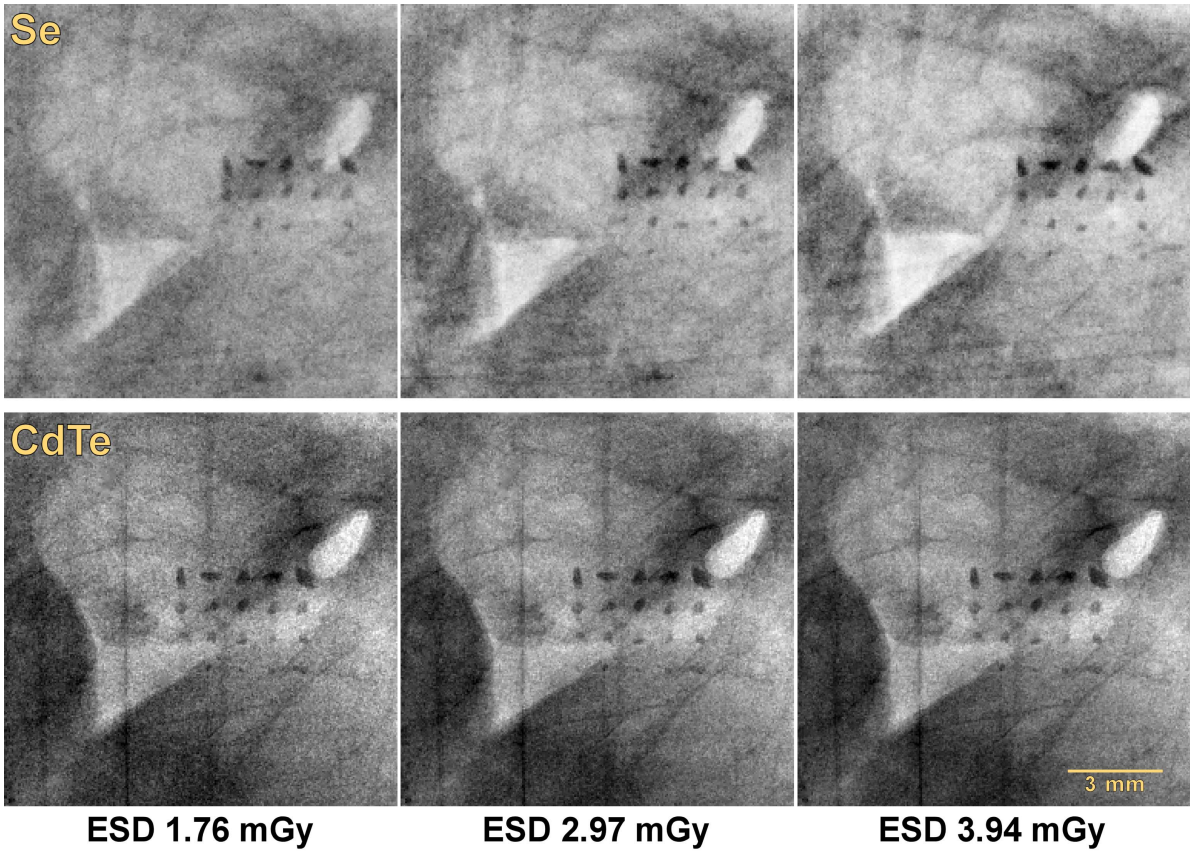

Fig. 8. Radiography comparison of the human breast tissue phantom between the Se-detector and CdTe-detector at three different entrance surface doses: 1.76 ± 0.05 mGy, 2.97 ± 0.04 mGy and 3.94 ± 0.12 mGy. The measured image quality of the CdTe-Medipix3RX is higher than of the Se-detector.

resolution- and contrast-loss because of the scaling of the image size. For the comparison, three different ESD were used: 1.76 ± 0.05 mGy, 2.97 ± 0.04 mGy and 3.94 ± 0.12 mGy. The highest dose is the standard value used in the clinical system; the medium dose corresponds to 75 % and the lowest to 45 % of the standard dose. For each ESD the CdTe-sensor images show a significantly higher spatial resolution and contrast than the a-Se-detector. The visibility of tiny structures like the smallest visible HA-crystals is better with the CdTe-Medipix3RX. Regarding the visibility of small structures, the image quality of the CdTe-Medipix3RX is at the lowest dose already comparable to the standard dose with the a-Se-detector.

For quantification of the benefit of the CdTe-Medipix3RX detector against the a-Se-detector, the CNR of HA-crystals was calculated. Two HA-crystal sizes were selected as the region of interest: the smallest visible crystals with 125-250 μm diameter average size (47 pixels), and the largest crystals with 500 μm in diameter (333 pixels). For defining the ROI, only the crystals were selected, without surrounding background. For the background, a homogenous white tissue area (189 pixels) was selected. Due to the slight movement of the phantom between the measurements, only crystals with the same background were selected for CNR calculation, and only the same crystals for all detectors to achieve directly comparable CNR values. Besides the nearest-neighbor interpolation for dead pixels, strictly no image processing was performed for the CdTe-Medipix3RX and the Si-Medipix3RX. The image output of the a-Se-detector is processed directly by the Hologic X-ray system, but no information about processing is available.

As shown in Fig. 9 the CNR for large HA-crystals with a diameter $\geq$ 500 μm is increasing with dose, as expected. The CNR increase for the a-Se-detector is higher than for the Si-Medipix3RX. The slope of the CdTe-Medipix3RX is similar to the a-Se-detector, except for an offset. Due to the higher attenuation efficiency of the CdTe-detector and its higher spatial resolution, superior CNR values are reached with lower doses than with the a-Se-detector. There is a drop in the CNR gain at around 80 % of the standard dose because of temporal stability issues of the CdTe-sensor. Due to the high leakage current of 30 μA of this sensor, the counting behavior of the detector is changing rapidly [49] and negatively influences the achievable CNR. If a small percentage of pixels is significantly changing its counting behavior during the acquisition time window, as is the current case, there is a noticeable influence on the CNR of small structures such as HA-crystals. Because of recent improvements in the processing of CdTe, it is now possible to produce such a CdTe-sensor with a magnitude lower leakage current of 2 - 3 μA [50]. Such an improved CdTe-sensor is significantly more stable regarding count rate changes over time; therefore, an even higher CNR will be

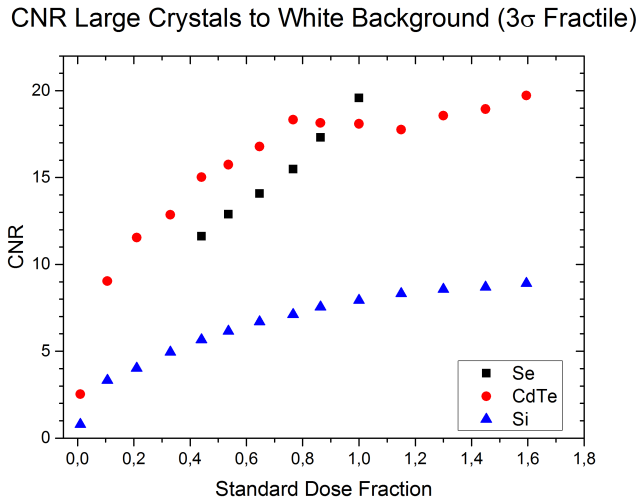

Fig. 9. CNR comparison of large HA-crystals with a size > 500 μm, measured with 200 μm Se-detector, 1 mm CdTe-Medipix3RX and 500 μm Si-Medipix3RX. The CdTe-Medipix3RX detector shows the highest CNR, but also a plateauing from 80 % of the standard dose because of stability issues of the CdTe-sensor material, which was not observed for Si.

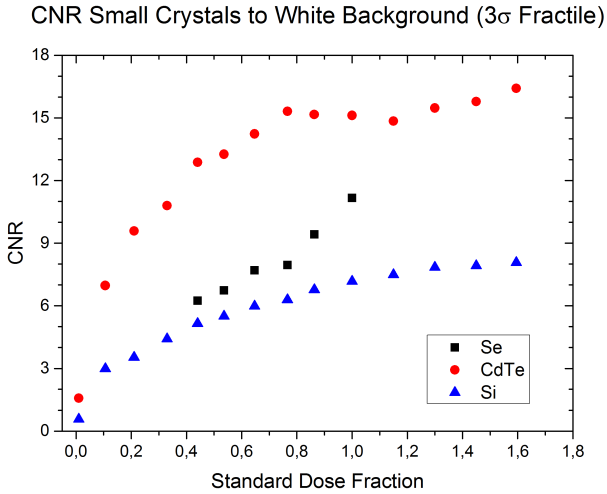

Fig. 10. CNR comparison of small HA-crystals with a size in the range 125 - 250 μm, measured with 200 μm Se-detector, 1 mm CdTe-Medipix3RX and 500 μm Si-Medipix3RX. Due to the higher spatial resolution and the higher attenuation efficiency, the CNR of the CdTe-Medipix3RX detector is superior to the other detectors.

possible. The CNR of the Si-Medipix3RX is not competitive with the other two detectors because of the low attenuation efficiency of the Si sensor.

The benefit of the CdTe-Medipix3RX for mammography is even more pronounced if very small structures are considered. Fig. 10 shows the CNR for small HA-crystals with a diameter of 125 – 250 μm. The CNR values of the CdTe-Medipix3RX are significantly higher than those of the other two detectors due to the combination of high spatial resolution with high attenuation efficiency. Because of the limited spatial resolution of the a-Se-detector, the CNR values are closer to the Si-Medipix3RX than to the CdTe-Medipix3RX. Due to the stability issue of the CdTe-sensor above 80 % of the standard dose, the CNR of the CdTe-Medipix3RX is plateauing the same way as for the CNR of the large crystals. A higher CNR is possible if a more stable CdTe-sensor is used.

D. Comparison With Related Work

A comparison of multiple direct converting high-Z sensor materials for mammography was shown by Tümer *et al.* [51]. A non-photon counting CCD ASIC was used as readout chip in combination with CdZnTe, GaAs, Se and PbI_2 sensors. Quantitative DQE/MTF results have been shown for CdZnTe only, but no characterization measurements for the sensor materials GaAs, Se and PbI_2. For these materials, only high kVp raw images of hard contrast objects were shown. The measured spatial resolution of the CdZnTe detector was comparable to the spatial resolution measured in this work due to the use of very thin 150 μm and 200 μm CdZnTe sensors in combination with the small pixel pitch of 50 μm of the ASIC. Other publications compare either CdTe/CdZnTe or GaAs with standard sensor materials and are not cross-comparable due to different measurement conditions, ASIC types and analysis methods employed.

Due to the higher attenuation efficiency of GaAs in the mammography energy range, compared to CdTe/CdZnTe [52], GaAs is a prominent sensor material in research on photon counting mammography detectors. First experiments have been carried out with Medipix1 detectors with 200 μm thick GaAs sensors by Amendolia *et al.* [53], [54] and Bisogni *et al.* [55]. The achieved spatial resolution was lower in comparison to this work caused by the large pixel pitch of 170 μm of the Medipix1 detector. Due to the threshold value of 11 keV used by the detector, the measured DQE was also low. Annovazzi *et al.* [56] and Amendolia *et al.* [57] presented CNR values for low-contrast phantoms. In both publications, the achieved contrast was significantly lower than the results presented in this work. An ABIX photon counting ASIC with a pixel pitch of 75 μm and a 500 μm GaAs sensor was used by Gkoumas *et al.* [58]. It was found that the MTF and DQE both depend on the detector threshold, but the impact of the threshold setting was lower than the one measured in this work. One reason is the larger pixel pitch of the detector, resulting in a decrease of charge sharing caused by X-ray fluorescence. Because of the larger pixel pitch, the achieved spatial resolution was lower than in this study.

Alsager and Spyrou [59] performed Monte-Carlo simulations for a 500 μm CdZnTe sensor with 50 μm and 100 μm pixel pitch detectors using a 28 kVp mammography spectrum. They found that the MTF of the 50 μm pixel pitch detector is more affected by charge sharing than that of the 100 μm pixel pitch detector, and that the MTF of a CdZnTe sensor is comparable to a CdTe sensor. The influence of the leakage current of the sensor was not simulated. Pani *et al.* [60] used a HEXITEC ASIC with 250 μm pixel pitch and a 1 mm thick CdTe sensor for contrast-enhanced breast imaging. It was found that the use of contrast agents in mammography requires higher X-ray tube voltages of up to 50 kVp for an optimum CNR. The obtained X-ray images show more noisy pixels than Medipix3RX in this work. Suzuki *et al.* [61] and Okamoto *et al.* [62] simulated an energy selective, photon counting X-ray detector with 200 μm pixel pitch and a 1.5 mm thick CdTe sensor. It was stated that an increased X-ray tube voltage of 50 kVp in combination with energy weighting by the use of three energy bins could

lead to a dose reduction of around 10 % in comparison to a commercial Philips MicroDose SI mammography system, which is a lower reduction than the one presented in this work.

Bisogni *et al.* [55] used a Medipix2 detector with 55 μm pixel pitch and a 300 μm Si sensor and could detect HA crystals with a size of 320 μm or larger. Pfeiffer *et al.* [44] found that the lower pixel pitch of the Medipix2 detector in comparison to Medipix1, bump bonded to 300 μm thick Si sensors, significantly increases the spatial resolution, which is necessary for mammography. The smallest presented feature size was 0.8 mm. Blanchot *et al.* [63] compared a Medipix2-based mammography system with 700 μm thick Si-sensor with a Hologic Selenia system and found a better spatial resolution, but no quantitative measurements were presented.

The successful production of a mammography phantom, which is a hybrid of natural human tissue with artificial hydroxyapatite crystals in defined sizes, is a novelty presented in this study. Kiss *et al*. [64] and Willekens *et al*. [65] analyzed extracted human breast tissues containing microcalcifications, whose random size and spatial distribution would not allow an accurate size dependent CNR analysis, as the one in the present study.

IV. Conclusions and Outlook

In this study, the different sensor materials CdTe, GaAs and Si were bump bonded to the advanced photon counting Medipix3RX detector ASIC and compared, for the first time under identical conditions, for their practical suitability in mammography imaging by analysis of the CNR and spatial resolution of mammography phantoms.

The investigation of the optimum semiconductor sensor material for mammography showed that CdTe is giving the best performance regarding spatial resolution and contrast-to-noise ratio. Despite the slightly minor attenuation efficiency of CdTe versus GaAs in the mammography energy range, the achievable CNR is higher for CdTe due to the K-shell fluorescence of Ga and As. The yield for generation of GaAs fluorescences is very high in the mammography energy range. This is causing a blurring of the image, which can be prevented if the detector threshold is set above the K_α-energy of As (11.7 keV), but then the detection quantum efficiency (DQE) of the detector is significantly reduced and so is the CNR. In comparison to GaAs, the K-edges of Cd (26.7 keV) and Te (31.8 keV) are at the end of the mammography energy range, and only a small fraction of the X-ray spectrum is above these values. Even at the highest tube voltage setting of 32 kVp of standard mammography, only 1.5 % of the photons in the X-ray spectrum will generate Cd-K_α-fluorescence. For thick, dense breasts higher kVp-settings of 35 kVp can be useful in rare cases [66]. The amount of Cd-K_α- and Te-K_α-fluorescence here is still low with 4.2 %. Therefore, mammography radiographs acquired with CdTe-sensors are not substantially affected by K-shell fluorescence blurring.

The comparison between a clinical a-Se-detector and Medipix3RX detectors with Si- and CdTe-sensors showed that the achievable CNR is higher for the CdTe-Medipix3RX than for the a-Se-detector. The reasons for this result are complex. On the one hand, the photon counting principle of the Medipix3RX yields a higher CNR than for charge-integrating detectors. On the other hand, significantly lower proportion of K-shell fluorescence in CdTe- than in Se-sensors, which have very similar fluorescences to GaAs-sensors, results in images with higher spatial resolution. For tiny structures, like small calcifications, substantially higher CNR values can be achieved with the CdTe-sensors. A novelty is that even very small structures in the size of 125 - 250 μm could be detected reliably with high contrast. As the detection of small calcifications is an important demand for next generation mammography detectors, this work demonstrates for first time that the use of photon counting detectors with small pixel pitch and CdTe sensors can achieve this objective with a simultaneous, significant reduction of the radiation dose. The measurements in this work also show that Si-sensors are not suited very well for mammography measurements. Because of the low attenuation efficiency of Si, too many X-ray photons are not being registered with thin sensors, which are necessary for optimum spatial resolution.

Future work will address three main points. On the detector side, a new CdTe-Medipix3RX detector with an ohmic low leakage current sensor of 2 - 3 μA [50] will be produced. The lower leakage current will enable a better temporal stability with less counting fluctuations in detector pixels. This will allow for even higher CNR values than presented in this study. Furthermore, the possible benefit of energy-selective X-ray imaging with four energy bins of the Medipix3RX detector will be investigated in conjunction with the Charge Summing Mode CSM, which also requires a sensor with a low leakage current to ensure a high temporal stability and a high energy resolution. On the phantom side, a new human phantom will be built, which will not be frozen. In combination with a vertical X-ray measurement setup, a more stable behavior of the tissue will be achieved for a better direct comparison between different detectors. Finally, further measurements using the CdTe-Medipix3RX detector inside clinical X-ray mammography systems will be performed to analyze the influence of the X-ray tube, including a higher X-ray flux than in the laboratory setup, on the image quality.

Acknowledgment

The authors would like to express their thanks to the Clínica del Country in Bogotá, which made the comparison measurements with the Hologic Selenia mammography system possible. They would also like to thank Dr. E. Hamann for providing the “TOR MAM” mammography phantom and Dr. A. Fauler for bump bonding of the GaAs- and CdTe-Medipix detectors.

References

[1] D. L. Miglioretti *et al.*, “Radiation-induced breast cancer incidence and mortality from digital mammography screening: A modeling study,” *Ann. Internal Med.*, vol. 164, no. 4, pp. 205–214, Jan. 2016.

[2] M. C. Jansen-van der Weide, M. J. W. Greuter, L. Jansen, J. C. Oosterwijk, R. M. Pijnappel, and G. H. de Bock, “Exposure to low-dose radiation and the risk of breast cancer among women with a familial or genetic predisposition: A meta-analysis,” *Eur. Radiol.*, vol. 20, no. 11, pp. 2547–2556, Nov. 2010.

[3] Mammography Quality Standards Act, U. S. Food & Drug Administration, USA. (Sep. 2019). *MQSA Insights—MSQA National Statistics*. [Online]. Available: https://www.fda.gov/radiation-emitting-products/mqsa-insights/mqsa-national-statistics

[4] M. A. Durand, "Synthesized mammography: Clinical evidence, appearance, and implementation," *Diagnostics*, vol. 8, no. 2, p. 22, Apr. 2018.

[5] R. E. Hendrick, "Radiation doses and cancer risks from breast imaging studies," *Radiology*, vol. 257, no. 1, pp. 246–253, Oct. 2010.

[6] K. C. Young and J. M. Oduko, "Radiation doses received in the United Kingdom breast screening programme in 2010 to 2012," *Brit. J. Radiol.*, vol. 89, no. 1058, pp. 1–13, 2016.

[7] E. Samei, R. S. Saunders, J. A. Baker, and D. M. Delong, "Digital mammography: Effects of reduced radiation dose on diagnostic performance," *Radiology*, vol. 243, no. 2, pp. 396–404, May 2007.

[8] D. O'Leary and L. Rainford, "Can radiation dose in mammography be further reduced by increasing the image quality?" *Breast Cancer Res.*, vol. 13, no. S1, p. P21, Dec. 2011.

[9] J. B. McCullagh, P. Baldelli, and N. Phelan, "Clinical dose performance of full field digital mammography in a breast screening programme," *Brit. J. Radiol.*, vol. 84, no. 1007, pp. 1027–1033, Nov. 2011.

[10] X. J. Rong *et al.*, "Microcalcification detectability for four mammographic detectors: Flat-panel, CCD, CR and screen/film," *Med. Phys.*, vol. 29, no. 9, pp. 2052–2061, Sep. 2002.

[11] A. Noel and F. Thibault, "Digital detectors for mammography: The tech-nical challenges," *Eur Radiol*, vol. 14, no. 11, pp. 1990–1998, Nov. 2004.

[12] T.-T. Kuo, C.-M. Wu, I. Chan, H.-H. Lu, and S.-H. Pao, "Direct-conversion X-ray detector with 50-μm high-gain pixel amplifiers for Low-X-ray-dose digital mammography," *J. Med. Biol. Eng.*, vol. 35, no. 2, pp. 249–257, Apr. 2015.

[13] M. J. Yaffe, "Detectors for digital mammography," in *Digital Mammography* (Medical Radiology), U. Bick and F. Diekmann, Eds. Berlin, Germany: Springer, 2010.

[14] P. M. Fralliciardi, J. Jakubek, D. Vavrik, and J. Dammer, "Comparison of single-photon counting and charge-integrating detectors for X-ray high-resolution imaging of small biological objects," *Nucl. Instrum. Methods Phys. Res. A, Accel. Spectrom. Detect. Assoc. Equip.*, vol. 607, no. 1, pp. 221–222, Aug. 2009.

[15] K. F. Pfeiffer, *Evaluation of the Medipix Detectors for Medical X-Ray Imaging, With Special Consideration of Mammography*. Erlangen, Germany: Univ. Nürnburg-Erlangen, 2004.

[16] M. Sarajlić *et al.*, "Development of edgeless TSV X-ray detectors," *J. Instrum.*, vol. 11, no. 2, Feb. 2016, Art. no. C02043.

[17] J. Jakubek *et al.*, "Large area pixel detector WIDEPIX with full area sensitivity composed of 100 timepix assemblies with edgeless sensors," *J. Instrum.*, vol. 9, no. 4, Apr. 2014, Art. no. C04018.

[18] S. O. Kasap and J. A. Rowlands, "Direct-conversion flat-panel X-ray image sensors for digital radiography," *Proc. IEEE*, vol. 90, no. 4, pp. 591–604, Apr. 2002.

[19] A. Rodríguez-Ruiz, M. Castillo, J. Garayoa, and M. Chevalier, "Evaluation of the technical performance of three different commercial digital breast tomosynthesis systems in the clinical environment," *Phys. Medica*, vol. 32, no. 6, pp. 767–777, Jun. 2016.

[20] *Selenia Dimensions With AWS 5000—A Flexible Platform for the Next Dimension in Breast Imaging*, Hologic Inc., Marlborough, MA, USA, 2011.

[21] M. Overdick *et al.*, "Status of direct conversion detectors for medical imaging with X-rays," *IEEE Trans. Nucl. Sci.*, vol. 56, no. 4, pp. 1800–1809, Aug. 2009.

[22] R. Ballabriga *et al.*, "The Medipix3RX: A high resolution, zero dead-time pixel detector readout chip allowing spectroscopic imaging," *J. Instrum.*, vol. 8, no. 2, Feb. 2013, Art. no. C02016.

[23] *Medipix3 Collaboration at CERN*. Accessed: Jan. 23, 2020. [Online]. Available: https://medipix.web.cern.ch/collaboration/medipix3-collaboration

[24] R. Ballabriga *et al.*, "Review of hybrid pixel detector readout ASICs for spectroscopic X-ray imaging," *J. Instrum.*, vol. 11, no. 1, Jan. 2016, Art. no. P01007.

[25] X. Llopart, R. Ballabriga, M. Campbell, L. Tlustos, and W. Wong, "Timepix, a 65k programmable pixel readout chip for arrival time, energy and/or photon counting measurements," *Nucl. Instrum. Methods Phys. Res. A, Accel. Spectrom. Detect. Assoc. Equip.*, vol. 581, nos. 1–2, pp. 485–494, Oct. 2007.

[26] N. Tartoni *et al.*, "Excalibur: A three million pixels photon counting area detector for coherent diffraction imaging based on the Medipix3 ASIC," in *Proc. IEEE Nucl. Sci. Symp. Med. Imag. Conf. Rec. (NSS/MIC)*, Anaheim, CA, USA, Oct. 2012, pp. 530–533.

[27] W. C. Barber, J. C. Wessel, E. Nygard, and J. S. Iwanczyk, "Energy dispersive CdTe and CdZnTe detectors for spectral clinical CT and NDT applications," *Nucl. Instrum. Methods Phys. Res. A, Accel. Spectrom. Detect. Assoc. Equip.*, vol. 784, pp. 531–537, Jun. 2015.

[28] T. Takahashi and S. Watanabe, "Recent progress in CdTe and CdZnTe detectors," *IEEE Trans. Nucl. Sci.*, vol. 48, no. 4, pp. 950–959, Aug. 2001.

[29] M. Z. Kabir and S. Kasap, "Photoconductors for X-ray image detectors," in *Springer Handbook of Electronic and Photonic Materials* (Springer Handbooks), S. Kasap and P. Capper, Eds. Cham, Switzerland: Springer, 2017.

[30] S. Procz, J. Lubke, A. Zwerger, M. Mix, and M. Fiederle, "Optimization of Medipix-2 threshold masks for spectroscopic X-ray imaging," *IEEE Trans. Nucl. Sci.*, vol. 56, no. 4, pp. 1795–1799, Aug. 2009.

[31] S. Procz *et al.*, "Flatfield correction optimization for energy selective X-ray imaging with Medipix3," *IEEE Trans. Nucl. Sci.*, vol. 58, no. 6, pp. 3182–3189, Dec. 2011.

[32] D. Vavrik, T. Holy, J. Jakubek, S. Pospisil, Z. Vykydal, and J. Dammer, "X-ray micro radiography using beam hardening correction," in *Proc. IEEE Nucl. Sci. Symp. Conf. Rec.*, Fajardo, Puerto Rico, Oct. 2005, pp. 2989–2992.

[33] (2014). *TOR MAM Mammography Phantom*. [Online]. Available: https://www.leedstestobjects.com/

[34] L. Nolting, P. Hunt, T. Cook, and B. Douglas, "An inexpensive and easy ultrasound phantom," *J. Ultrasound Med.*, vol. 35, no. 4, pp. 819–822, Apr. 2016.

[35] C. Avila, L. Mendoza, G. Roque, L. Loaiza, J. Racedo, and R. Rueda, "Feasibility study of a TIMEPIX detector for mammography applications," *Proc. SPIE*, vol. 10572, Nov. 2017, Art. no. 105720Z.

[36] J. S. Calderón-García, G. A. Roque, and C. A. Ávila, "Construction of mammography phantoms with a 3D printer and tested with a TIMEPIX system," *Proc. SPIE*, vol. 10572, Nov. 2017, Art. no. 105720Y.

[37] V. Kraus, M. Holik, J. Jakubek, M. Kroupa, P. Soukup, and Z. Vykydal, "FITPix—Fast interface for timepix pixel detectors," *J. Instrum.*, vol. 6, no. 1, Jan. 2011, Art. no. C01079.

[38] H.-E. Nilsson, C. Frojdh, and E. Dubaric, "Monte Carlo simulation of charge sharing effects in silicon and GaAs photon counting X-ray imaging detectors," in *Proc. IEEE Nucl. Sci. Symp. Conf. Rec.*, Portland, OR, USA, 2003, pp. 1401–1404.

[39] D. R. Dance, "Physical principles of mammography," in *Physics for Medical Imaging Applications*, Y. Lemoigne, A. Caner, and G. Rahal, Eds. Dordrecht, The Netherlands: Springer, 2007, pp. 355–365.

[40] D. R. Dance, A. K. Thilander, M. Sandborg, C. L. Skinner, I. A. Castellano, and G. A. Carlsson, "Influence of anode/filter material and tube potential on contrast, signal-to-noise ratio and average absorbed dose in mammography: A Monte Carlo study.," *Brit. J. Radiol.*, vol. 73, no. 874, pp. 1056–1067, Oct. 2000.

[41] I. Han, M. Şahin, L. Demir, and Y. Şahin, "Measurement of K X-ray fluorescence cross-sections, fluorescence yields and intensity ratios for some elements in the atomic range 22≤Z≤68," *Appl. Radiat. Isot.*, vol. 65, no. 6, pp. 669–675, Jun. 2007.

[42] M. Zuber, T. Koenig, E. Hamann, A. Cecilia, M. Fiederle, and T. Baumbach, "Characterization of a 2×3 timepix assembly with a 500 μm thick silicon sensor," *J. Instrum.*, vol. 9, no. 5, May 2014, Art. no. C05037.

[43] E. Hamann *et al.*, "Performance of a Medipix3RX spectroscopic pixel detector with a high resistivity gallium arsenide sensor," *IEEE Trans. Med. Imag.*, vol. 34, no. 3, pp. 707–715, Mar. 2015.

[44] K.-F.-G. Pfeiffer, J. Giersch, and G. Anton, "How good is better? A comparison between the Medipix1 and the Medipix2 chip using mammographic phantoms," *Nucl. Instrum. Methods Phys. Res. A, Accel. Spectrom. Detect. Assoc. Equip.*, vol. 531, nos. 1–2, pp. 246–250, Sep. 2004.

[45] J. Crocco *et al.*, "Study of the effects of edge morphology on detector performance by leakage current and cathodoluminescence," *IEEE Trans. Nucl. Sci.*, vol. 58, no. 4, pp. 1935–1941, Aug. 2011.

[46] D. D. Duarte *et al.*, "Edge effects in a small pixel CdTe for X-ray imaging," *J. Instum.*, vol. 8, no. 10, pp. 1–14, Oct. 2013.

[47] G. Anton *et al.*, "Imaging theory for X-ray pixel detectors," *Nucl. Instrum. Methods Phys. Res. A, Accel. Spectrom. Detect. Assoc. Equip.*, vol. 563, no. 1, pp. 116–123, Jul. 2006.

[48] J. Marchal, "Theoretical analysis of the effect of charge-sharing on the Detective Quantum Efficiency of single-photon counting segmented silicon detectors," *J. Instrum.*, vol. 5, no. 1, Jan. 2010, Art. no. P01004.
[49] S. Procz, "Hochauflösende computertomographie mit Medipix3-halbleiterdetektoren," Ph.D. dissertation, Universität Freiburg, Freiburg im Breisgau, Germany, 2012.
[50] S. Elbracht-Leong, "MYTHEN CdTe: A new generation MYTHEN CdTe: A new generation state-of-the-art X-ray imaging detector," Ph.D. dissertation, School Phys., Univ. Melbourne, Melbourne, VIC, Australia, Jun. 2016, p. 58.
[51] T. O. Tümer *et al.*, "High-resolution pixel detectors for second generation digital mammography," *Nucl. Instrum. Methods Phys. Res. A, Accel. Spectrom. Detect. Assoc. Equip.*, vol. 497, no. 1, pp. 21–29, Jan. 2003.
[52] S. R. Amendolia *et al.*, "A prototype for a mammographic head and related developments," *Nucl. Instrum. Methods Phys. Res. A, Accel. Spectrom. Detect. Assoc. Equip.*, vol. 518, nos. 1–2, pp. 382–385, Feb. 2004.
[53] S. R. Amendolia *et al.*, "Test of a GaAs-based pixel device for digital mammography," *Nucl. Instrum. Methods Phys. Res. A, Accel. Spectrom. Detect. Assoc. Equip.*, vol. 460, no. 1, pp. 50–54, Mar. 2001.
[54] S. R. Amendolia *et al.*, "Characterization of a mammographic system based on single photon counting pixel arrays coupled to GaAs X-ray detectors," *Med. Phys.*, vol. 36, no. 4, pp. 1330–1339, Mar. 2009.
[55] M. G. Bisogni *et al.*, "A Medipix2-based imaging system for digital mammography with silicon pixel detectors," *IEEE Trans. Nucl. Sci.*, vol. 51, no. 6, pp. 3081–3085, Dec. 2004.
[56] A. Annovazzi *et al.*, "A GaAs pixel detectors-based digital mammographic system: Performances and imaging tests results," *Nucl. Instrum. Methods Phys. Res. A, Accel. Spectrom. Detect. Assoc. Equip.*, vol. 576, no. 1, pp. 154–159, Jun. 2007.
[57] S. R. Amendolia *et al.*, "Low contrast imaging with a GaAs pixel digital detector," *IEEE Trans. Nucl. Sci.*, vol. 47, no. 4, pp. 1478–1482, Aug. 2000.
[58] S. Gkoumas, T. Thuering, A. Taboada, A, Jensen, M. Rissi, and C. Broennimann, "Dose-independent near-ideal DQE of a 75 μm pixel GaAs photon-counting spectral detector for breast imaging," *Proc. SPIE* vol. 10948, Mar. 2019, Art. no. 109480V.
[59] A. A. Alsager and N. M. Spyrou, "Evaluation of image performance of CZT detector for digital mammography: Monte Carlo simulation," *Nucl. Instrum. Methods Phys. Res. A, Accel. Spectrom. Detect. Assoc. Equip.*, vol. 580, no. 1, pp. 462–465, Sep. 2007.
[60] S. Pani *et al.*, "High energy resolution hyperspectral X-ray imaging for low-dose contrast-enhanced digital mammography," *IEEE Trans. Med. Imag.*, vol. 36, no. 9, pp. 1784–1795, Sep. 2017.
[61] R. Suzuki *et al.*, "A proposed new image display method with high contrast-to-noise ratio using energy resolved photon-counting mammography with a CdTe series detector," *Proc. SPIE*, vol. 10573, Mar. 2018, Art. no. 105735K.
[62] C. Okamoto *et al.*, "Discrimination between normal breast tissue and tumor tissue using CdTe series detector developed for photon-counting mammography," *Proc. SPIE*, vol. 9783, Mar. 2016, Art. no. 97832G.
[63] G. Blanchot *et al.*, "Dear-Mama: A photon counting X-ray imaging project for medical applications," *Nucl. Instrum. Methods Phys. Res. A, Accel. Spectrom. Detect. Assoc. Equip.*, vol. 569, no. 1, pp. 136–139, Dec. 2006.
[64] M. Z. Kiss, D. E. Sayers, Z. Zhong, C. Parham, and E. D. Pisano, "Improved image contrast of calcifications in breast tissue specimens using diffraction enhanced imaging," *Phys. Med. Biol.*, vol. 49, no. 15, pp. 3427–3439, Aug. 2004.
[65] I. Willekens *et al.*, "High-resolution 3D micro-CT imaging of breast microcalcifications: A preliminary analysis," *BMC Cancer*, vol. 14, no. 1, Jan. 2014.
[66] P. Bernhardt, T. Mertelmeier, and M. Hoheisel, "X-ray spectrum optimization of full-field digital mammography: Simulation and phantom study," *Med. Phys.*, vol. 33, no. 11, pp. 4337–4349, Nov. 2006.